Chemical Physics Letters 631–632 (2015) 97–102

Contents lists available at ScienceDirect

Chemical Physics Letters

journal homepage: www.elsevier.com/locate/cplett

Superconductivity in bulk polycrystalline metastable phases of Sb_2Te_3 and Bi_2Te_3 quenched after high-pressure–high-temperature treatment

S.G. Buga [a,b,*], V.A. Kulbachinskii [b,c,d], V.G. Kytin [c], G.A. Kytin [c], I.A. Kruglov [b], N.A. Lvova [a,b], N.S. Perov [c], N.R. Serebryanaya [a,b], S.A. Tarelkin [a], V.D. Blank [a,b]

[a] Technological Institute for Superhard and Novel Carbon Materials, 142190 Troitsk, Moscow, Russia
[b] Moscow Institute of Physics and Technology, 141700 Dolgoprudny, Moscow Region, Russia
[c] M.V. Lomonosov Moscow State University, Low Temperature Physics Department, 119991 Moscow, Russia
[d] Moscow Engineering Physics Institute (MEPhI) – National Nuclear Research University, 115409 Moscow, Russia

ARTICLE INFO

Article history:
Received 11 December 2014
In final form 28 April 2015
Available online 11 May 2015

ABSTRACT

We synthesized bulk polycrystalline samples of metastable phases of Sb_2Te_3 and Bi_2Te_3 topological insulators by rapid quenching after a high-pressure–high-temperature treatment at $P = 3.7–7.7$ GPa; $T = 873$ K and found superconducting transitions with $T_C^{onset} = 2$ K and 6 K, respectively. A low critical current value of about 2 mA in the metastable Sb_2Te_3 phase and an absence of the detectable heat capacity effect at the superconducting transition indicated a low-dimensional character of superconductivity. A zero-field magnetic susceptibility cusp and linear positive magnetoresistance indicate a topological insulator state.
© 2015 Elsevier B.V. All rights reserved.

1. Introduction

Bismuth and antimony tellurides and selenides like Bi_2Te_3, Sb_2Te_3, Bi_2Se_3, Sb_2Se_3 refer to 3D-type topological insulators (TIs) – materials with an odd number of Dirac cones in the energy spectrum of the surface charge carriers [1–4]. This peculiarity arises due to a particular crystal structure and electronic configuration of the surface atoms in TIs. Among other unusual electronic and magnetic properties, TIs may possess the unconventional p-wave superconductivity. In such a case, topological insulators promise the route for making topological quantum computing systems based on Majorana fermions – quasiparticles with non-Abelian statistics [5,6]. The unconventional odd-parity bulk superconductivity was found in Sr_2RuO_4 and $Sn_{1-x}In_xTe$ compounds [7,8]. Recent studies on the effects of Bi_2Se_3 TI doping with copper [9–11] and high-pressure treatment of pure Bi_2Se_3 [12] revealed some signs of unconventional superconductivity in this selenide. But unlike the Cu-doped samples, pure Bi_2Se_3 possesses superconductivity only "in situ" under pressure above 10 GPa [12,13]. The high-pressure superconducting phases have been also found in the other TIs like Bi_2Te_3 [14,15], Sb_2Te_3 [16], and Sb_2Se_3 [17] and in indium tellurides like In_3Te_4, In_2Te_3 [18]. However, the transitions to superconducting phases were reversible, similarly to Bi_2Se_3, after the pressure release they transformed back to non-superconducting phases. Research on the correlation of the superconductivity with the topological quantum effects and practical applications of the materials directly under high pressure is very complicated. Thus, there is a strong demand to create materials displaying both topological insulator properties and superconductivity at normal pressure.

Unlike the previous studies, we applied a combined high-pressure–high-temperature (HPHT) treatment with the subsequent rapid cooling to quench the high-pressure structures of antimony and bismuth tellurides [19–21]. We found two metastable Sb_2Te_3 phases by quenching after treatment at $P = 4$ GPa; $T = 873$ K and at $P = 7.7$ GPa; $T = 873$ K. The former of them, defined as m-Sb_2Te_3, is quite stable at ambient conditions. Its crystal structure is monoclinic (C2/m) with the unit cell dimensions: $a = 15.644(80)$ Å, $b = 4.282(8)$ Å, $c = 9.382(20)$ Å, $\beta = 89.70(5)^\circ$. We described the atomic model of this structure in [21]. The structure of the metastable Bi_2Te_3 phase quenched after treatment at $P = 7.7$ GPa; $T = 973$ K is rhombohedral ($R3m$), the unit cell parameters are: $a = 4.42$ Å, $b = 29.84$ Å [19]. We indicate this structure as m-Bi_2Te_3.

Now, in this Letter we investigated for the first time the superconductivity and topological insulator properties of the bulk

* Corresponding author at: Technological Institute for Superhard and Novel Carbon Materials, 142190 Troitsk, Moscow, Russia.
E-mail addresses: buga@tisnum.ru, sergei7a@yandex.ru (S.G. Buga).

http://dx.doi.org/10.1016/j.cplett.2015.04.056
0009-2614/© 2015 Elsevier B.V. All rights reserved.

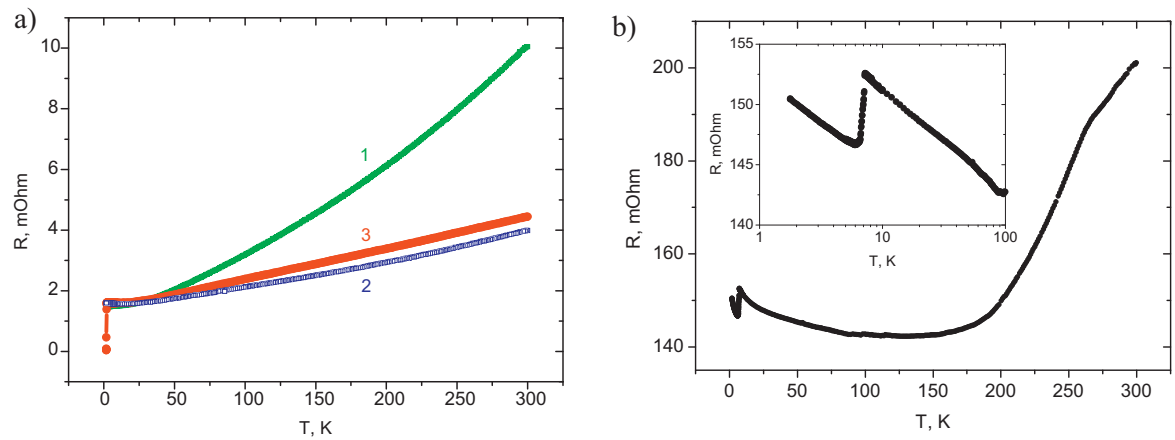

Figure 1. Temperature dependencies of electrical resistance of Sb_2Te_3 samples (a) and m-Bi_2Te_3 phase (b). 1 – pristine crystalline Sb_2Te_3 in *ab*-plane; 2 – polycrystalline Sb_2Te_3 quenched after HPHT treatment at $P = 3.5$ GPa: $T = 873$ K; 3 – polycrystalline α-Sb_2Te_3 quenched after HPHT treatment at $P = 4$ GPa: $T = 873$ K.

polycrystalline samples of m-Sb_2Te_3 and m-Bi_2Te_3 metastable phases quenched after HPHT treatment, and calculated the band structure of the bulk of an optimized m-Sb_2Te_3 phase.

2. Materials and methods

We used the commercially available high-purity (99.999%) Sb_2Te_3 and Bi_2Te_3 alloys. Both of them have a rhombohedral $R\bar{3}m$ structure [22]. We have synthesized the m-Sb_2Te_3 and m-Bi_2Te_3 metastable high-pressure phases by rapid quenching after the electrical current thermoresistive heating in an "anvil with cavity"-type high-pressure apparatus [19,23]. The high-pressure–high-temperature experiments were carried out up to a 7.7 GPa pressure with heating up to 1123 K. The sample cooling rate was ≈60°/min, and its pressure reduction rate in the reaction cell ≈1 GPa per minute. The output samples were 2.2 mm thick and 6.0 mm in diameter.

For the analysis of the crystal structure and physical properties of the samples, we employed the powder X-ray diffraction, electrical, magnetic, and heat capacity measurements as well as ab initio calculations.

We studied the temperature dependencies of the electrical resistivity of the samples via a conventional 4-probe method down to 0.45 K, their current–voltage characteristics, effect of magnetic field up to 9 T and heat capacity by differential scanning calorimetry in the temperature range of 1.8–300 K using the Quantum Design® physical properties measurement system (PPMS).

The ab initio calculations involving the density functional theory were performed to calculate the electronic density of states DOS and the band structure of the optimized metastable α-Sb_2Te_3 phase. We carried out the optimization of atomic positions at fixed cell parameters determined from the experimental X-ray diffraction data [21] which were similar to the ones published in [24]. Calculations of the electronic density of states (DOS) and band structure were performed using the Vienna Ab initio Simulation Package (VASP) [25]. The Perdew–Burke–Ernzerhof exchange-correlation according to [24] and the projector-augmented wave method with a 300 eV kinetic energy cutoff were used. The coordinates of the high-symmetry **k**-path in the Brillouin zone of the monoclinic lattice were selected for the electronic band structure according to [26].

3. Experimental results

Temperature dependencies of the electrical resistance for the initial single-crystal Sb_2Te_3 sample and polycrystalline samples obtained by quenching under high pressure of 3.5 GPa; 3.7 GPa and 4 GPa after heating up to $T = 873$ K exhibit a typical metal-like behavior: the resistance increases approximately linearly with a temperature in the range of 30–300 K, and varies slightly in the range of 2–30 K (Figure 1a). However, it should be noted that the Hall coefficient is positive in the initial Sb_2Te_3 (dominating hole conductivity), and it is negative in the m-Sb_2Te_3 samples (electron-type conductivity). We observed superconductivity below $T = 2$ K in the m-Sb_2Te_3 samples (Figure 1a, curve 3 and Figure 2a), while it was not observed in the sample treated at $P = 3.5$ GPa; $T = 873$ K with the initial rhombohedral structure type (Figure 1a, curve 2). The width of superconducting transition in the m-Sb_2Te_3 samples is fairly narrow – 0.2 K. The global superconductivity took place at $T < 1.8$ K.

The magnetic field shifts an onset of the superconductivity temperature with the rate of $\alpha = -0.32\ \mathrm{T\,K^{-1}}$ (Figure 2a). The value of the critical current is very small: only 2 mA at $T = 1.76$ K (Figure 3a). At this current value, the superconductivity onset was observed only at $T = 1.2$ K, and the global superconductivity occurred at $T < 0.5$ K (Figure 3b). The IV-characteristic in Figure 3a shows a typical Josephson junction effect. The transverse magnetoresistance is positive and increases linearly with the magnetic field at $H > 25$ kOe by a factor of 0.35% $\mathrm{kOe^{-1}}$ (Figure 4a).

A differential scanning calorimetry study of the heat capacity did not show a characteristic peak at the superconductivity transition temperature, which could indicate the bulk nature of superconductivity.

Only a weak superconductivity effect with a 96% residual resistance takes place in the m-Bi_2Te_3 phase at $T < 7$ K (Figure 1b). The ratio of the superconductivity onset temperature on the magnetic field is equal to $-0.4\ \mathrm{T\,K^{-1}}$. The transverse magnetoresistance effect is positive and linear on the magnetic field value, as well as in the case of Sb_2Te_3 samples, but the magnitude of the relative change of resistance is substantially less than 0.1% $\mathrm{kOe^{-1}}$ (Figure 4b). A sharp increase in the resistance in the field less than 1 T occurs due to destruction of superconductivity.

We investigated the magnetic moment of the m-Sb_2Te_3 phase and the single-crystal sample with a pristine structure as a function of magnetic field in the range of −20 to 20 kOe at room temperature (Figure 5a). Within the measurement accuracy of 10^{-6} emu, we did not see a deviation of the field dependence of magnetization from diamagnetic behavior in the pristine Sb_2Te_3 sample. The measured diamagnetic susceptibility value of pristine single-crystal Sb_2Te_3 was about $-0.36 \times 10^{-6}\ \mathrm{emu\,g^{-1}}$. Unlike that, the polycrystalline m-Sb_2Te_3 samples show a paramagnetic additive (Figure 5b). Susceptibility showed a characteristic topological insulator zero-field cusp [27].

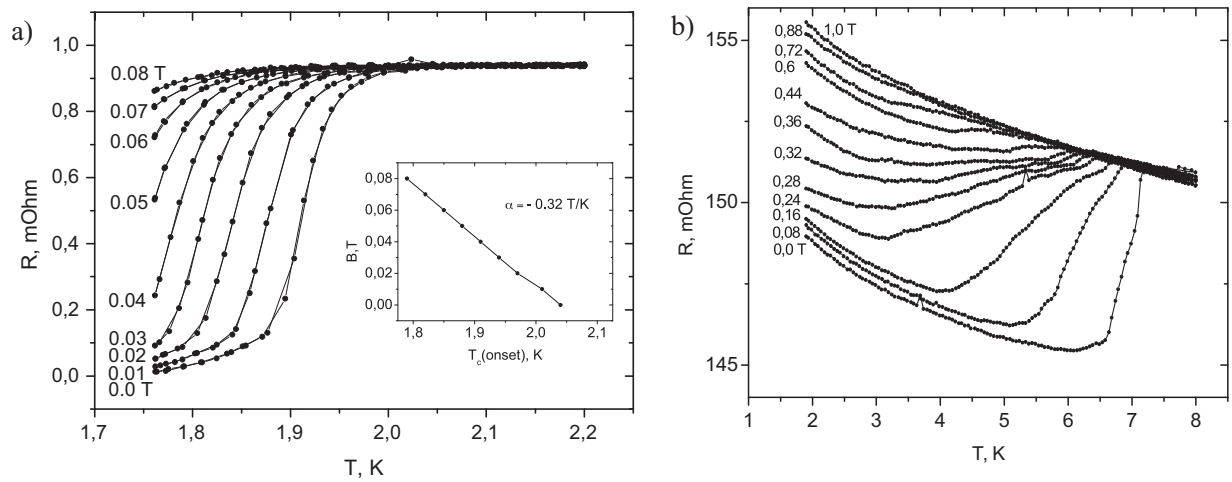

Figure 2. Magnetic field effect on superconductivity transition temperature in α-Sb_2Te_3 phase (a) and m-Bi_2Te_3 phase (b). The insert shows the superconductor phase diagram.

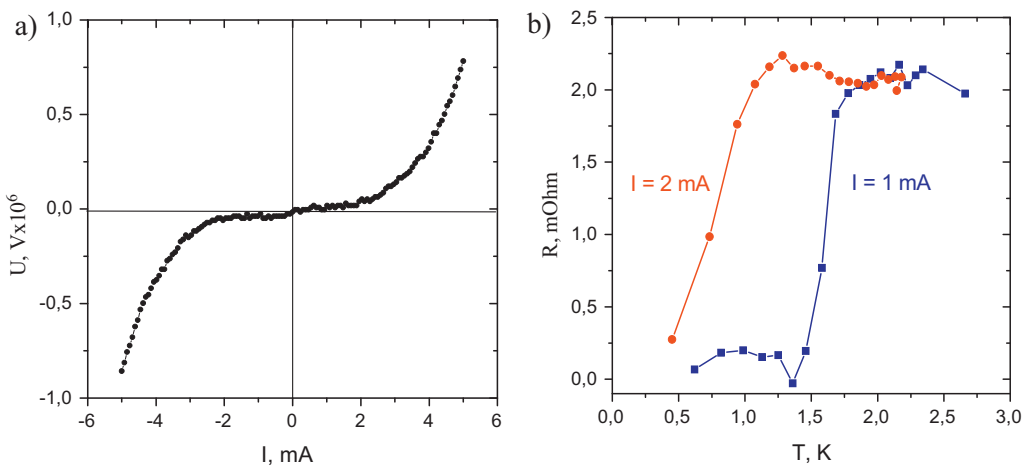

Figure 3. Current–voltage (I–U) characteristic of m-Sb_2Te_3 phase at $T = 1.76$ K (a) and temperature shift of the superconductivity transition at 1 mA and 2 mA electrical current (b). The solid lines serve as a guide for eyes.

3.1. *The electronic density of states and the band structure of m-Sb_2Te_3*

In Figure 6a and b we show the results of calculation of bulk DOS for the initial Sb_2Te_3 phase and for the metastable m-Sb_2Te_3 phase. It is evident that unlike semiconductor bulk of the equilibrium phase, the bulk of m-Sb_2Te_3 phase is semimetallic. There are two local maxima of the valence band top above the Fermi level, and two local minima of the conduction band bottom below it. The Dirac cone in the surface states energy spectrum may be located

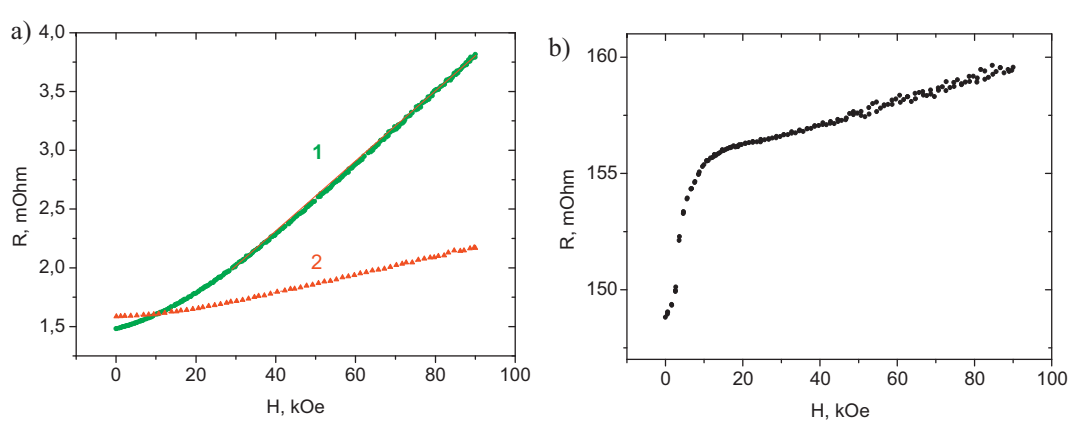

Figure 4. Linear transverse magnetoresistance effect in Sb_2Te_3 (a) and m-Bi_2Te_3 samples (b) at $T = 2$ K: 1 – pristine crystalline Sb_2Te_3, current in *ab*-plane; 2 – polycrystalline m-Sb_2Te_3 phase.

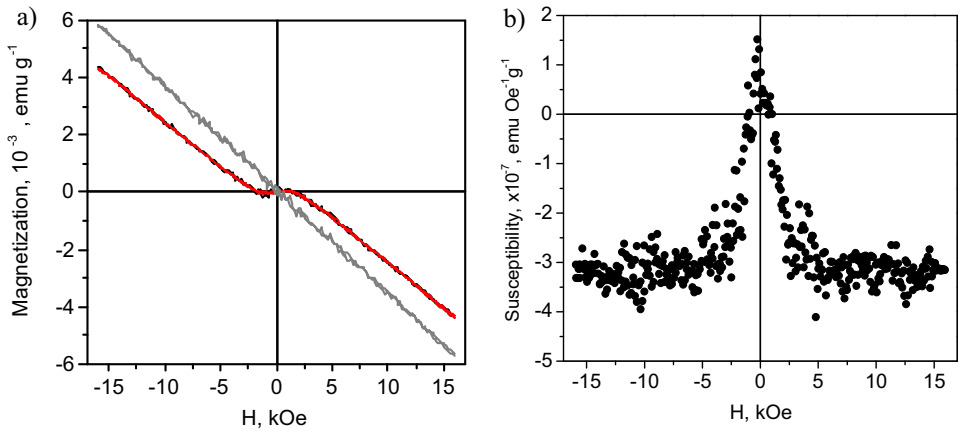

Figure 5. Magnetic moment of the pristine single-crystal Sb_2Te_3 (*gray*) and m-Sb_2Te_3 phase (*red*) vs magnetic field at room temperature (a). Susceptibility of m-Sb_2Te_3 phase vs magnetic field (b).

in the center of the Brilluen zone (point G in Figure 6c) as in the pristine phase, and additionally in 4 equivalent points between X and M. Thus, an odd number of Dirac cones in the Brilluene zone may take place. Transition to a metallic type of the energy spectrum in a bulk of m-Sb_2Te_3 is consistent with its structure: interatomic distances in the metastable phase are proper to the metallic bonds [28]. And the appearance of the metallic-type bonding correlates with the experimentally observed electron-type conductivity of the m-Sb_2Te_3 phase, unlike dominating hole-type conductivity in the initial one [19,21].

4. Discussion

The observed superconductivity effects in the quenched metastable phases of Sb_2Te_3 and Bi_2Te_3 topological insulators are much similar to the data obtained "*in situ*" under the high-pressure conditions in the range of 3–7 GPa [14–16]. However, the structures of the quenched phases and those observed under pressure are different. The electronic topological transitions at this pressure range and at room temperature were investigated in [29–31]. In those studies, the local minima in the lattice parameters ratio *c/a* have been observed at about 2–4 GPa, but no change in the type of structure was evaluated on the basis of XRD and Raman scattering data. We think that heating under pressure is a key factor for structural phase transitions into the metastable phases m-Sb_2Te_3 (with a monoclinic *C*2/*m* structure) and m-Bi_2Te_3 (with a rhombohedral *R*3*m* structure) which we revealed in [19–21]. In this article we describe superconductivity in the m-Sb_2Te_3 and m-Bi_2Te_3 phases at ambient pressure for the first time.

The *R*3*m* crystal structure of metastable phase of Bi_2Te_3 was determined first in [32]. Recently we repeated this study and determined the structure of m-Bi_2Te_3 phase [20]. The cell dimensions have changed a little with respect to the pristine phase: *a* increased by 0.02 Å, but *c* decreased by 0.6 Å. However the intensity of X-ray reflexes changed significantly. And so the structure is more in line with the *R*3*m* group with two Bi atoms positions and three Te atoms positions without center of symmetry. The metallic-like temperature drop of the electrical resistance in m-Bi_2Te_3 phase (Figure 1b)

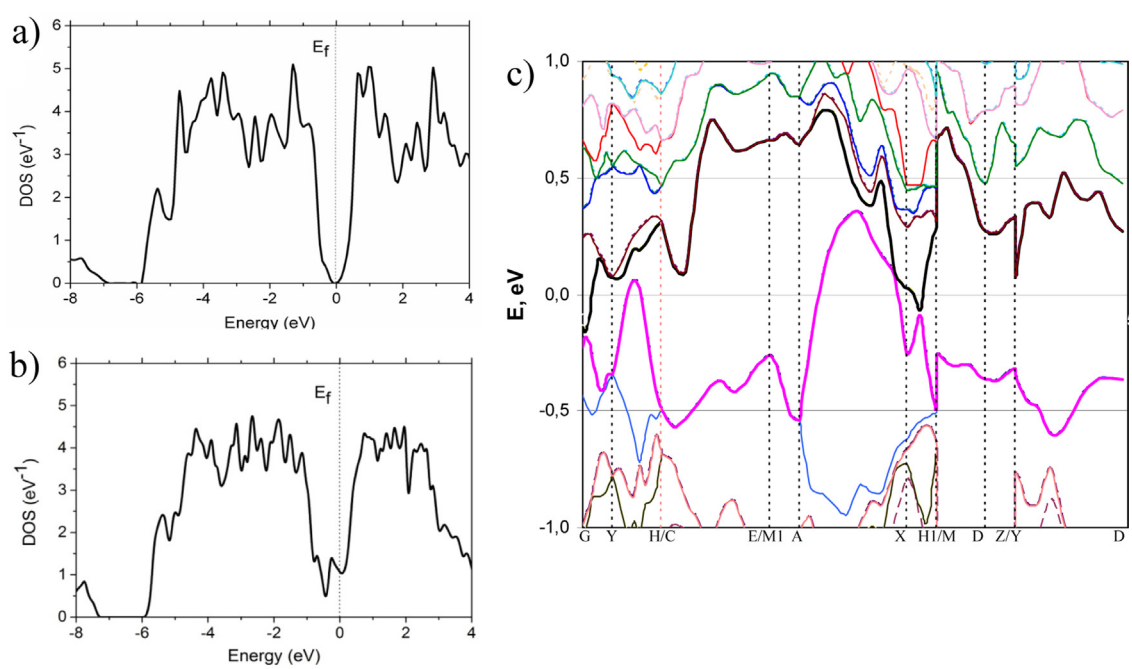

Figure 6. The calculated electronic density of states of equilibrium Sb_2Te_3 (a) and metastable α-Sb_2Te_3 (b) phases. (c) Band structure of the bulk of monoclinic m-Sb_2Te_3 phase.

may be a consequence of the substantial decrease in Te-Te distances. The diffraction pattern of the sample Bi_2Te_3 obtained "in situ" in a diamond-anvil cell at 4.4 GPa [30] is similar to m-Bi_2Te_3 pattern [20] and markedly different from the initial phase pattern. Thus, the structure of m-Bi_2Te_3 has no a symmetry center and its space group is $R3m$.

The observed low value of the critical superconductivity current of about 2 mA in m-Sb_2Te_3, and the strong dependence of the transition critical temperature on the electrical current value (Figure 3), as well as an absence of the heat capacity peak at superconductivity transition, indicate a two-dimensional nature of the superconducting channel. Such a two-dimensional superconductive layer in m-Bi_2Te_3 obviously is not continuous, thus a global superconductivity was not observed. The residual resistance at $T < T_c$ is relatively high.

We observed a nearly linear dependence of the resistance vs temperature (Figure 1a) and the linear dependence of the magnetoresistance vs magnetic field at $H > 20$ kOe (Figure 4a, curve 1) in the antimony telluride samples. A linear increase of the resistance along with temperature increase takes place due to an increase of the phonon scattering like in metals, semimetals, and degenerated semiconductors. The linear magnetoresistance (LMR) effect is typical in the topological insulators; however, a disorder in narrow-gap semiconductors also causes LMR [33]. In a case of polycrystalline samples obtained by quenching after HPHT treatment, the crystallographic orientation in the surface layer was random. Nevertheless, as one can see in Figures 1 and 3, the temperature dependencies of the resistance at $T > 2$ K and the magnetic field dependencies in the HPHT-treated samples are similar to the ones obtained on the basal face of the TI crystal with the initial structure. Unlike a bulk single-crystal pristine Sb_2Te_3, the magnetic susceptibility of the m-Sb_2Te_3 phase comprises both diamagnetic and paramagnetic compounds (Figure 5). Moreover, the paramagnetic compound definitely exhibits a zero-field cusp which is proper to a topological insulator state (Figure 5b). The calculation of the band structure and DOS for the optimized m-Sb_2Te_3 structure (Figure 6) indicates that it's bulk is semimetallic which is in agreement with the experimental R(T) function (Figure 1). The location of the Fermi level in the valence or conductivity band was observed experimentally in the doped bulk topological insulators, for example in [4,34,35]. Besides, we may assume that the real structure of the surface layer of the grains may differ from the bulk due to the reconstruction effects, and a thin surface layer may be a narrow-gap semiconductor with the Dirac cone in the energy spectrum. A more complicated modeling of the surface layer crystal structure of the m-Sb_2Te_3 phase and its band structure must be performed.

The upper critical field in the range of $H_{0C2} = 3$–5 T was measured in the cases of the copper-doped Bi_2Se_3 [11] and "in situ" under high pressure in pure Bi_2Se_3 [12], and such high numbers were considered as an indication of the p-wave superconductivity. Currently, we have been able to perform measurements of the critical magnetic field only at temperatures above 1.76 K which did not provide information about the upper critical field in the m-Sb_2Te_3 phase. A lower temperature range must be investigated.

The temperature dependence of resistivity in the bismuth telluride metastable phase m-Bi_2Te_3 sample also has a metallic character at $T > 200$ K, however, a weak increase in resistance with a temperature decrease was observed at $T < 150$ K (Figure 1b). Generally, residual resistance in a superconductivity temperature range may indicate a multiphase structure of the sample. Nevertheless, in a particular case of topological superconductivity, residual resistance may not evidence a multiphase nature of the sample. We suspect a 2D-type superconductivity on some definite faces of the grains of the polycrystal. A bulk of the grains and some intergrain boundaries may be nonsuperconductive, thus providing residual resistance. The magnetoresistance effect is positive like in Sb_2Te_3 and linear in a field $H > 10$ kOe, which is also proper to a topological insulator. A sharp increase of magnetoresistance in a magnetic field up to 10 kOe is due to the effect of destruction of superconductivity. Thus, the m-Sb_2Te_3, and m-Bi_2Te_3 phases possess topological insulator properties, similarly to the initial crystal and polycrystalline Sb_2Te_3 test samples.

5. Conclusion

We synthesized bulk polycrystalline samples of metastable phases of antimony and bismuth tellurides using a high-pressure and high-temperature treatment at $P = 3.7$–7.7 GPa; $T = 873$ K with subsequent quenching, and investigated their electrical and magnetic properties, in particular, their superconductivity transition. Unlike pristine structures, the quenched metastable phases of Sb_2Te_3 and Bi_2Te_3 possess superconductivity transition at normal pressure. A metastable Sb_2Te_3 phase is totally superconductive below $T_c = 1.75$ K, while a Bi_2Te_3 metastable phase has a residual resistance of about 96% below $T_c = 6$ K. We observed a linear positive transverse magnetoresistance effect in normal state and a zero-field paramagnetic cusp which are proper to topological insulators. The critical current value of the superconductivity in a metastable Sb_2Te_3 phase was very low – just about 2 mA. This fact and an absence of the detectible heat capacity effect at superconductivity transition indicate a low-dimensional character of the superconductivity.

The calculated DOS and the band structure of the bulk of optimized monoclinic metastable Sb_2Te_3 phase exhibit a semimetallic electronic structure, while some more complex calculations are required for modeling the crystal structure and the band structure of its surface layer.

Acknowledgements

The part of work made in FSBSU TISNCM was supported by the Ministry of Education and Science of the Russian Federation, grant 14.577.21.0090; the work was done using the Shared-Use Equipment Center of the Technological Institute for Superhard and Novel Carbon Materials.

References

[1] L. Fu, C.L. Kane, E.J. Mele, Phys. Rev. Lett. 98 (10) (2007) 106803.
[2] L. Fu, C.L. Kane, Phys. Rev. B 76 (4) (2007) 045302.
[3] H. Zhang, C.X. Liu, X.L. Qi, et al., Nat. Phys. 5 (2009) 438.
[4] Y.L. Chen, J.G. Analytis, J.-H. Chu, et al., Science 325 (2009) 178–180.
[5] C. Nayak, S.H. Simon, A. Stern, M. Freedman, S. Das Sarma, Rev. Mod. Phys. 80 (2008) 1083, http://dx.doi.org/10.1103/RevModPhys.80.1083
[6] L. Fu, C.L. Kane, Phys. Rev. Lett. 100 (2008) 096407.
[7] K.D. Nelson, Z.Q. Mao, Y. Maeno, Y. Liu, Science 306 (2004) 1151, http://dx.doi.org/10.1126/science.1103881
[8] S. Sasaki, Z. Ren, A.A. Taskin, K. Segawa, L. Fu, Y. Ando, Phys. Rev. Lett. 109 (2012) 217004.
[9] L.A. Wray, S.Y. Xu, Y. Xia, et al., Nat. Phys. 6 (2010) 855.
[10] S. Sasaki, M. Kriener, K. Segawa, et al., Rev. Lett. 107 (2011) 217001.
[11] T.V. Bay, T. Naka, Y.K. Huang, H. Luigjes, M.S. Golden, A. de Visser, Phys. Rev. Lett. 108 (2012) 057001.
[12] K. Kirshenbaum, P.S. Syers, A.P. Hope, et al., Phys. Rev. Lett. 111 (2013) 087001, http://dx.doi.org/10.1103/PhysRevLett.111.087001
[13] E.S. Itskevich, E.Ya. Atabaeva, S.V. Popova, Solid State Phys. 6 (1964) 1765.
[14] S.J. Zhang, J.L. Zhang, X.H. Yu, et al., J. Appl. Phys. 111 (2012) 112630.
[15] M.A. Il'ina, E.S. Itskevich, Sov. Phys. Sol. State 13 (1972) 2098.
[16] J. Zhu, J.L. Zhang, P.P. Kong, et al., Sci. Rep. 3 (2013) 2016, http://dx.doi.org/10.1038/srep02016
[17] P.P. Kong, F. Sun, L.Y. Xing, et al., Sci. Pep. 4 (2014) 6679, http://dx.doi.org/10.1038/srep06679/
[18] S. Geller, A. Jayaraman, G.W. Hull Jr., J. Phys. Chem. Sol. 26 (1965) 353.
[19] S.G. Buga, N.R. Serebryanaya, G.A. Dubitsky, E.E. Semenova, V.V. Aksenenkov, V.D. Blank, High Press. Res. 31 (1) (2011) 86.
[20] I.A. Kruglov, N.R. Serebryanaya, G.I. Pivovarov, V.D. Blank, Thermoelectricity 6 (2013) 35.
[21] N. Serebryanaya, E. Tatyanin, S. Buga, I. Kruglov, N. Lvova, V. Blank, Phys. Status Solidi 252 (2015) 267, http://dx.doi.org/10.1002/pssb.201451241

[22] R.W.G. Wyckoff, Crystal Structures, Krieger, Melbourne, FL, 1986, v.2.
[23] G.A. Dubitskiy, V.D. Blank, S.G. Buga, E.E. Semenova, V.A. Kul'bachinskii, A.V. Krechetov, V.G. Kytin, JETP Lett. 81 (6) (2005) 260.
[24] Y. Ma, G. Liu, P. Zhu, H. Wang, X. Wang, Q. Cui, J. Liu, Y. Ma, J. Phys.: Condens. Matter 24 (2012) 475403 (8pp).
[25] G. Kresse, J. Furthmüller, Phys. Rev. B 54 (1996) 11169.
[26] W. Setyawan, S. Curtarolo, Comput. Mater. Sci. 49 (2) (2010) 299.
[27] L. Zhao, H. Deng, I. Korzhovska, Z. Chen, M. Konczykowski, A. Hruban, V. Oganesyan, L. Krusin-Elbaum, Nat. Mater. 13 (2014) 3962.
[28] J.C. Slater, J. Chem. Phys. 41 (10) (1964) 3199.
[29] A. Nakayama, M. Einaga, Y. Tanabe, S. Nakanno, F. Ishikava, Y. Yamada, High Press. Res. 29 (2009) 245.
[30] A. Polian, M. Gauthier, S.M. Souza, D.M. Trichês, J.C. de Lima, T.A. Grandi, Phys. Rev. B 83 (2011) 113106.
[31] S.M. Souza, C.M. Poffo, D.M. Triches, J.C. de Lima, T.A. Grandi, A. Polian, M. Gauthier, Physica B 407 (2012) 3781.
[32] E.A. Atabaeva, E.C. Itskevich, S.A. Mashkov, et al., Fizika Tverdogo Tela 10 (1968) 43 (in Russian; English translation in Sov. Phys. Sol. State, 1968).
[33] M. Veldhorst, M. Snelder, M. Hoek, C.G. Molenaar, D.P. Leusink, A.A. Golubov, H. Hilgenkamp, A. Brinkman, Phys. Stat. Sol. 7 (2013) 26, http://dx.doi.org/10.1002/pssr.201206408
[34] Y. Xia, D. Qian, D. Hsieh, et al., Nat. Phys. 5 (2009) 398.
[35] Su-Yang Xu, Y. Xia, L.A. Wray, et al., Science 332 (2011) 560, http://dx.doi.org/10.1126/science.1201607.